Flow-induced aggregation of colloidal particles in viscoelastic fluids

Donglin Xie, Greg G. Qiao, and Dave E. Dunstan*
Department of Chemical and Biomolecular Engineering, The University of Melbourne, Parkville, Victoria 3010, Australia
(Received 2 May 2016; published 22 August 2016)

The flow-induced aggregation of dilute colloidal polystyrene nanoparticles suspended in Newtonian and viscoelastic solutions is reported. A rheo-optical method has been used to detect real-time aggregation processes via measuring optical absorption or scattering in a quartz Couette cell. The observed absorbance decreases over time are attributed to the flow-induced coagulation. Numerical simulations show that the aggregation processes still follow the Smoluchowski coagulation equation in a revised version. Suspensions in a series of media are studied to evaluate the effect of the media rheological properties on the particle aggregation. The data shows that elasticity reduces the aggregation while the solution viscosity enhances the aggregation processes.

DOI: 10.1103/PhysRevE.94.022610

I. INTRODUCTION

Nanomaterials show unique physical and chemical properties that are of great interest in a number of fundamental areas [1,2]. Many advanced materials in current and potential industrial applications are manufactured from nanoparticle suspensions [3,4]. A significant number of the applications, such as nanocomposites [3] and copolymer-nanoparticle mixtures [5], require processing from colloidal suspensions in polymeric and therefore viscoelastic media. The flow of the media affects the motion of the suspending particles [6,7], and hence the rheological property of the suspension [4,8,9], where the suspension stability is of great importance [10,11]. The manufacture and processing of devices from nanoparticle-polymer suspensions requires a detailed understanding of these systems in flow [3,5,12].

The coagulation of particles in viscous media has been previously studied and is believed to be dominated by the particle-particle interactions, particularly the traditional ones described by the Derjaguin, Landau, Verwey, Overbeek (DLVO) theory [10]. Recently, a series of works on shear-induced aggregation in strongly charge-stabilized aqueous colloids emphasized the effect of shear stress on nanoparticle aggregation [13–15]. However, in a number of works the hydrodynamic forces have been ignored or underestimated compared to the particle-particle interactions. Recent studies on suspensions in viscoelastic media, such as surfactant solutions and polymer solutions and melts, show that the viscoelastic nature of the suspending media influences the aggregation of suspending nanoscale particles [9,11]. Moreover, the non-DLVO interactions such as bridging, steric effect [16], and depletion force [17] need to be considered in suspensions containing polymers [10,18].

A number of studies have observed flow-induced aggregation for particles suspended in complex fluids [19–25]. The reason for the observed behavior is not fully understood [12,20,21,24,26]. Particle aggregation and/or flow-induced alignment of microscale particles in viscoelastic media has been reported in a series of flow types, such as cone and plate flows [19,20], simple (or oscillatory) shear flows [21,22], plane-Poiseuille flows [23], and torsional flows [24]. At low shear rates, a long string-like structure oriented in the flow direction was observed to form on shear startup; while if the shear rate was large enough, the segments join abreast to form aggregates that are relatively short and wide [22,24,25]. Additionally, a number of experiments on two spherical particle systems indicate that there are attractive interactions between particles moving in viscoelastic fluids but not in Newtonian fluids [27–29]. A body of research has been directed to determining the factors causing this aggregation (or alignment). In the early papers, Michele *et al.* [21] and Feng *et al.* [24] postulated that the physical origin of this particle alignment was associated with normal stress effects. Later, Scirocco *et al.* [20] and Won *et al.* [26] only observed the alignment in shear-thinning viscoelastic fluids rather than Boger fluids, which indicated the shear thinning resulted in the alignment. The key research question of fundamental importance in understanding the observed phenomena is whether the viscosity and/or elasticity lead to the flow-induced aggregation. To date there are still no quantitative ways to justify the influence of viscosity and elasticity on particle aggregation in flow.

In this paper, we study the flow-induced aggregation of colloidal latex nanoparticles suspended in Newtonian and non-Newtonian media using a rheo-optical technique [30] that utilizes optical absorption spectrophotometry. We attempt to distinguish between the effects of Newtonian viscosity, elasticity, and shear thinning on shear-induced aggregation for these systems in order to develop a deeper physical insight into this problem. Real-time spectra were collected in the sheared dilute suspensions. Numerical simulations based on the Smoluchowski coagulation equation and Mie theory determine a collisional coefficient (see theory section below) that enables the evaluation of the effects of viscosity and elasticity on the particle aggregation.

II. MATERIALS AND METHODS

The suspending fluids were selected with the objective to investigate the viscoelastic effects, thus a series of solutions with different polyacrylamide concentrations and water-glycerol proportions were prepared. Polyacrylamide (Separan AP30, supplied from Dow Chemical Ltd, U.S.A.) was first dissolved in double-distilled water, of which the corresponding molecular weight is reported as 3.1 million, respectively [31]. Then

*davided@unimelb.edu.au

TABLE I. Compositions of the suspending media.

Sample	c_{AP30} (ppm)	c_{Na^+} (ppm)	Solvent (water/glycerol w/w)	n_{ri}
AP30-50-1	100	1.02	50/50	1.399
AP30-50-2	200	2.00	50/50	1.399
AP30-50-4	400	4.69	50/50	1.399
AP30-60-2	200	2.10	60/40	1.384
AP30-70-2	200	2.04	70/30	1.372
Control-1	0	0	34.5/65.5	1.442
Control-2	0	2.02	34.5/65.5	1.442
Control-3	0	4.03	34.5/65.5	1.442
Control-4	0	6.05	34.5/65.5	1.442

glycerol (analytical reagent, supplied from Chem Supply) was added to vary the viscosity ranges. The solutions were then placed on the stirring platform at room temperature (25°C) for 2.5 h to mix properly. The detailed compositions of the suspending solutions are listed in Table I.

Rheological properties of the solutions were measured using an ARES rheometer with a Couette geometry (of which the inner diameter is 32 mm, the outer diameter is 34 mm, and the radius to gap ratio is 16:1) at room temperature (25°C). The viscosity η was measured in the steady-state mode over shear rate range from 1/s to 1000/s as shown in Fig. 1. The storage modules G' and loss modules G'' were then measured in the oscillation mode with a constant 10.0% strain. The G' value decreasing in the AP30-50-1 solution at frequencies over 70 Hz is due to the inertia limitation of the instrument and the linear region of the solution.

The impurities in Separan AP30 (largely NaCl) introduced sodium ions into the viscoelastic solutions. An Agilent inductively coupled plasma optical emission spectrometry (ICP-OES) was used to measure the Na^+ concentration in each solution and also confirm that there was no other ionic contaminations in the solution. As listed in Table I, a series of Newtonian fluids with different concentrations of NaCl (analytical reagent, supplied from Chem Supply) were made as control solutions. Additionally, the solution refractive index n_{ri} was measured via an Abbe 60 refractometer at room temperature (25°C).

As a dispersed phase, polystyrene nanoparticles (surfactant-free white sulfate latex from Interfacial Dynamics Corp., with $d = 0.2\,\mu$m) were used to make the measured suspensions. This was verified by dynamic light scattering (DLS) measurement that the latex nanoparticles were monodisperse and their average diameter was $d_0 = 2r_0 = 212 \pm 7$ nm. The latex nanoparticles were dispersed properly in the suspensions via a Bronson 1210 ultrasonic cleaner for 20 min. A constant particle volume fraction $\phi = 3.3\times10^{-4}$ was used in all the suspensions reported herein. All the suspensions could be stored at room temperature (25°C) for several days without showing any signs of aggregation or sedimentation.

A Cary 3E spectrophotometer was used to collect the ultraviolet and visible absorption spectra of the latex particle suspensions from 200 to 700 nm (the black curve in Fig. 3) with a maximum at 228 nm. The suspensions are loaded inside the quartz Couette geometry as shown in Fig. 2. The detailed dimensions and experimental setup used is similar to that reported previously [7]. The shear rates in the experiment range from 0 to 1000/s, and the calculations of the Reynolds number and Taylor number indicates that the flow system is laminar and free of recirculating vortices:

$$\mathrm{Re} = \frac{\dot{\gamma} d R}{\eta/\rho} < 1500 < 2100 = \mathrm{Re}_c, \tag{1}$$

$$\mathrm{Ta} = \frac{\dot{\gamma}^2 d^5}{R(\eta/\rho)^2} < 20 < 1700 = \mathrm{Ta}_c. \tag{2}$$

III. THEORY

The radius of the spherical particles used in the suspensions is 106 nm. In the measured wavelength range from 200 to 700 nm, the scattered light can be described accurately using Mie scattering theory [32]. For dilute spherical particle (radius r) suspensions, the scattering cross section is

$$c_{\mathrm{ext}} = \frac{2\pi}{k^2}\sum_{n=1}^{\infty}(2n+1)\mathrm{Re}\{a_n + b_n\}, \tag{3}$$

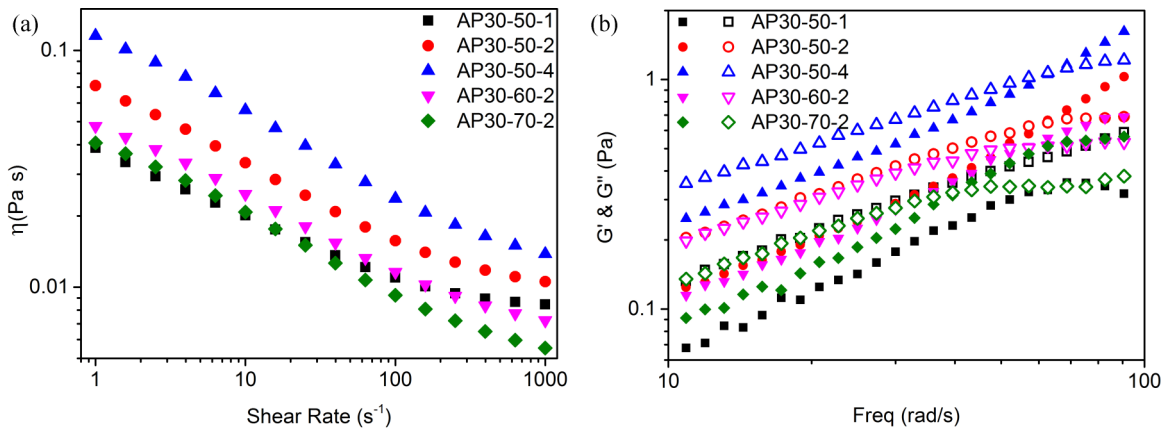

FIG. 1. (a) Viscosity and (b) G' (solid) and G'' (hollow) versus shear rate and frequency of the solutions used in the experiments.

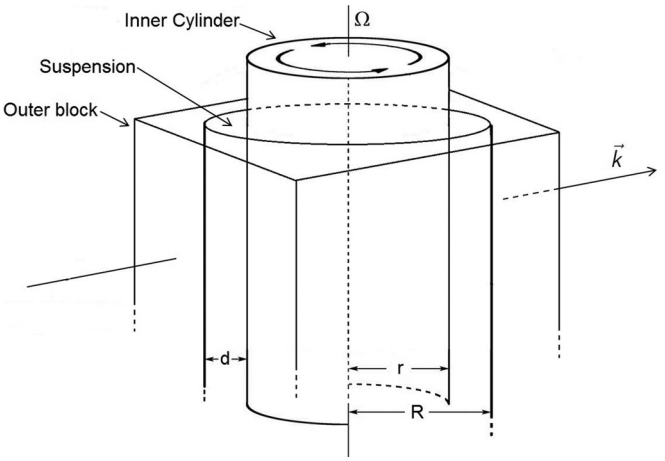

FIG. 2. Schematic of optical Couette flow apparatus ($r = 4.90$ mm, $R = 5.00$ mm) [7].

and

$$a_n = \frac{\psi_n(x)\psi_n'(mx) - m\psi_n'(x)\psi_n(mx)}{\zeta_n^{(1)}(x)\psi_n'(mx) - m\zeta_n^{(1)\prime}(x)\psi_n(mx)}, \tag{4}$$

$$b_n = \frac{\psi_n'(x)\psi_n(mx) - m\psi_n(x)\psi_n'(mx)}{\zeta_n^{(1)\prime}(x)\psi_n(mx) - m\zeta_n^{(1)}(x)\psi_n'(mx)}, \tag{5}$$

where λ is the wavelength of incident light, $x = kr = 2\pi Nr/\lambda$ is the size parameter, $m = N_1^*/N$ is the relative refractive index (N_1^* and N are the refractive indices of the particle and medium, respectively), and the functions $\psi_n(x)$ and $\zeta_n^{(1)}(x)$ are Riccati-Bessel functions. The complex refractive indices of the latex beads are assumed to be the same as those of the bulk polystyrene, of which the imaginary parts (extinction coefficient) are measured by Inagaki *et al.* [33] and the real parts are calculated via the Kramers-Kronig relation,

$$N_1(E) - 1 = \frac{2}{\pi}\int_0^\infty \frac{E'K_1(E')}{E'^2 - E^2}dE', \tag{6}$$

where E is the photon energy of the incident light, and $K_1(E)$ is the extinction coefficient.

The Beer-Lambert law relates the particle extinction cross section c_{ext} to the observed absorbance,

$$I_{\text{Abs}} = c_{\text{ext}}nl, \tag{7}$$

where n is the number density of particles, and l the laser path length through the samples. The absorbance spectrum of the latex beads in the AP30-50-2 suspension is simulated via Mie theory [the red curve in Fig. 3(a)], which is in a good agreement with the experimental result [the black curve in Fig. 3(a)]. Moreover, the volume fraction $\phi(=4n\pi r^3/3)$ of the suspending particles is constant in the rheo-optic experiments. The absorbance can be represented as

$$I_{\text{Abs}} = \frac{3\phi l c_{\text{ext}}}{4\pi r^3}, \tag{8}$$

which means that the radius of the attenuating clusters can be calculated from the measured absorbance directly.

Based on the Smoluchowski coagulation equation, the collision rate has a factor two times the macroscopic number concentration of particles in the system. Zaccone *et al.* [13] expressed the kinetic equation for the rate of change of the concentration of particles in Newtonian media as

$$\frac{dn}{dt} = -\kappa' n^2 \tag{9}$$

and

$$\kappa' \sim \frac{1}{\eta}\sqrt{\frac{3\pi\alpha\eta\dot{\gamma}r_0^3 - U_m''}{k_BT}}e^{-(U_m - 6\pi\alpha\eta\dot{\gamma}r_0^3)/k_BT}, \tag{10}$$

where α is a numerical coefficient depending on the flow type; U_m is the interaction barrier (or the interaction-potential maximum, and $U_m'' < 0$, respectively), which is determined by the particle-particle interactions and should be constant for a given set of suspension conditions.

Integrating Eq. (9), we can get

$$\frac{1}{n} - \frac{1}{n_0} = \kappa'(t - t_0), \tag{11}$$

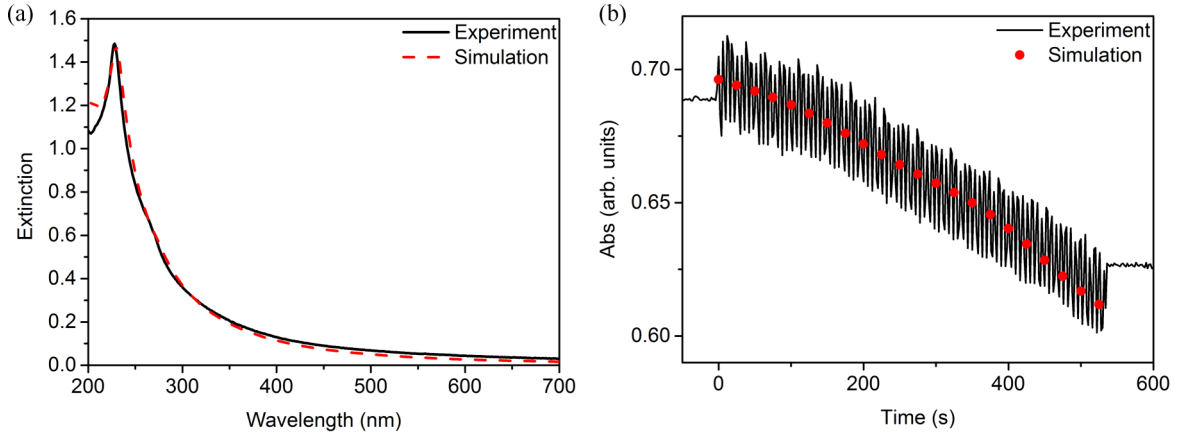

FIG. 3. (a) Normalized UV and visible absorption spectra of the AP30-50-2 suspension (the solvent background has been subtracted) experimentally (black line) and simulatively (red dash line). (b) Absorbance (at 250 nm) changes with time in the Couette flow of 282/s experimental (black curve) and simulation (red dots).

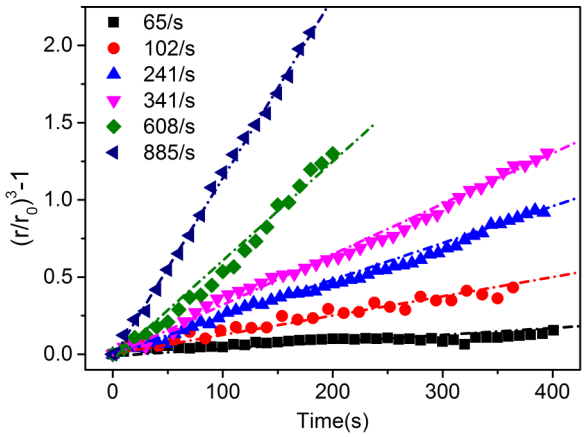

FIG. 4. The aggregation radius versus time in the AP30-50-2 suspension under the Couette flows with different shear rates.

then substitute $n = 3\phi/4\pi r^3$ into the equation,

$$\left(\frac{r}{r_0}\right)^3 - 1 = \frac{3\phi\kappa'}{4\pi r_0^3}(t - t_0) = \kappa(t - t_0), \tag{12}$$

where the aggregation rate κ is expressed by

$$\kappa = \frac{3\phi}{4\pi r_0^3}\kappa' \sim \frac{1}{\eta}\sqrt{\frac{3\pi\alpha\eta\dot{\gamma}r_0^3 - U_m''}{k_BT}}e^{-(U_m - 6\pi\alpha\eta\dot{\gamma}r_0^3)/k_BT}. \tag{13}$$

κ increases with the shear stress $\sigma = \eta\dot{\gamma}$ in an exponential trend. Eq. (13) can be rewritten as

$$\ln(\kappa\eta) \sim \frac{6\pi\alpha r_0^3}{k_BT}\sigma - \frac{U_m}{k_BT} + \frac{1}{2}\ln\left(\frac{3\pi\alpha\sigma r_0^3 - U_m''}{k_BT}\right), \tag{14}$$

where an approximately linear relationship between aggregation rate κ and shear stress σ is given when the shear stress is large enough ($\sigma > k_BT/30\pi\alpha r_0^3$):

$$\ln(\kappa\eta) \sim \frac{6\pi\alpha r_0^3}{k_BT}\sigma. \tag{15}$$

As shown in Eq. (10), only the effect of viscous stress is considered on the aggregation kinetics. In order to incorporate the viscoelastic effect, we introduce a coefficient ξ into Eq. (15),

$$\ln(\kappa\eta) = \xi\sigma + \Lambda, \tag{16}$$

where Λ is a constant for a certain suspension. For Newtonian fluids, $\xi = 6\pi\alpha r_0^3/k_BT$ is a constant that is only determined by the flow type and original particle radius. However, for viscoelastic media, ξ can no longer have the same expression due to the presence of elasticity and shear thinning. By comparing ξ among different suspensions, we are able to evaluate the viscoelastic effect on the shear-induced aggregation.

IV. RESULTS AND DISCUSSION

In Fig. 3, an experimental kinetic spectrum of the AP30-50-2 suspension in the Couette flow of 282/s is collected with the incident light at 250 nm. When flow is applied, the absorption intensity oscillates (resulting from small spatial mismatches between the motor system and the flow cell), while a decreasing trend of the absorbance over time is observed. Based on Eq. (8), the absorbance decrease indicates that the radius of the suspending particles rises in this suspension, namely an aggregation of the latex beads occurs in flow. The best numerical fitting for this kinetic spectrum from Eq. (12) is plotted as the red dots in Fig. 3(b) with $\kappa = 3.51\times10^{-3}$.

A series of Couette shear rates were applied to the AP30-50-2 suspensions with the shear rates varying from ~60/s to ~900/s. The measured kinetic spectra were smoothed to eliminate the oscillation deviations due to the experimental system. Then the kinetic absorption spectra were converted to the average aggregation radius that changes over time using Mie theory. In Fig. 4, the radius-time curves are plotted in the coordinate $[(r/r_0)^3 - 1]$ versus time. The coagulation of the latex nanoparticles occurs in both low and high shear rate flows. It was observed that the cluster size increases more rapidly in the higher shear rates. Importantly, linear relationships are observed in Fig. 4, which is in good agreement with the theoretical analysis of Eq. (12). Thus, the κ values are interpreted via the best linear fits as shown in Fig. 4.

The rheo-optical experiments were conducted on all the Newtonian and non-Newtonian suspensions listed in Table I. Similar phenomena are observed, and for each experiment, a κ value is obtained via the same method discussed above. As shown in Eq. (16), the κ values in the coordinate are

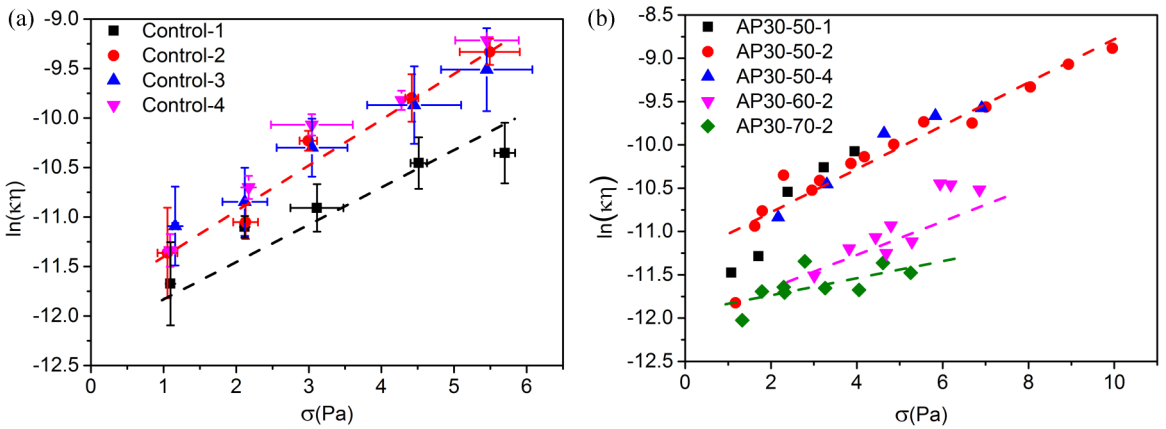

FIG. 5. $\ln(\kappa\eta)$ versus σ in the (a) Newtonian and (b) non-Newtonian suspensions.

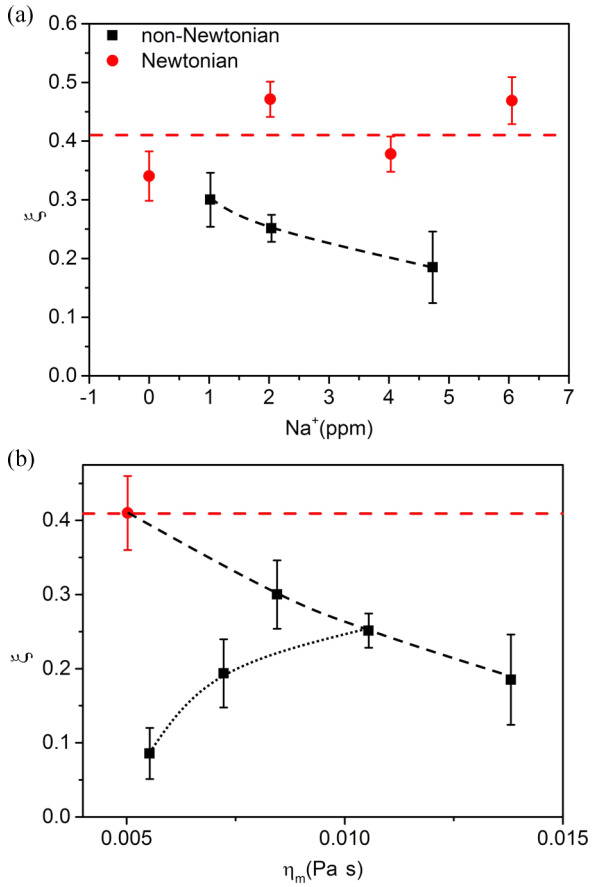

FIG. 6. (a) ξ versus sodium ions concentration in AP30-50-X series suspensions (black squares) and Newtonian suspensions (red dots). (b) ξ versus η_m: black dash line for AP30-50-X series samples and black dot line for AP30-X0-2 series samples; the red dashed line is for Newtonian suspensions and the red circle represents the Newtonian suspension with the same water-glycerol fraction as the AP30-50-X series samples.

plotted as $\ln(\kappa\eta) - \sigma$, where the viscosity is calculated from Fig. 1 using linear interpolation for each suspension. In Fig. 5, the linear relationship between $\ln(\kappa\eta)$ and σ is within the experimental error for all suspensions measured. This indicates that the assumption made in Eq. (16) is proper and reasonable. Additionally, the ξ value for each suspension can be calculated from the slope in Fig. 5.

In Fig. 6(a), the ξ versus Na^+ concentrations for both Newtonian and non-Newtonian suspensions is plotted. ξ in Newtonian suspensions is nearly constant with various Na^+ concentrations, showing that the Na^+ impurity should have little effect on the ξ. As listed in Table I, the Na^+ concentrations are proportional to the polymer concentrations in the AP30-50-X series samples with the same water-glycerol fraction. The decrease of ξ in the AP30-50-X series samples is not due to the Na^+ concentration, but the varying polymer concentration. For the polymer concentration increase leads to a rise in the elasticity of the fluids, the elasticity is shown to significantly reduce the observed flow induced aggregation.

Though the effect of viscosity on aggregation has been considered at each shear rate in Eq. (13) and Fig. 5, the shear thinning makes it difficult to directly compare the different media. Here we introduce η_m, the lower-limit viscosity of shear-thinning viscoelastic fluids, to evaluate the effect of the solution viscosity and use the viscosity at 1000/s, respectively, when plotting ξ over η_m in Fig. 6(b). For the Newtonian suspensions, the ξ value is independent of the viscosity as shown in Eq. (15), which is plotted as the red dash line in Fig. 6(b). Therefore, an extra point can be added to the AP30-50-X series samples, of which the Newtonian suspending medium has the same water-glycerol fraction but does not contain any polyacrylamide. In the AP30-X0-2 series samples, the value of ξ increases with the viscosity, which indicates that the aggregation accelerates in the suspension with large η_m. However, the opposite trend is observed in the AP30-50-X series samples which confirms that the suspension elasticity has the reduction effect on the aggregations.

V. CONCLUSIONS

In conclusion, the flow-induced aggregation of polystyrene nanoparticles occurs in both Newtonian and non-Newtonian media. The real-time aggregation processes were measured using a rheo-optical technique that utilizes both Couette flow and optical absorbance. Using Mie theory, we found the Smoluchowski coagulation equation is able to describe the aggregation process. Furthermore, the coefficient ξ was used to evaluate the viscoelastic effect on the aggregation. The measured aggregation accelerates in the suspensions with large η_m and the elasticity largely eliminates the flow induced aggregation processes. Further verification of these findings for other polymer-nanoparticle systems will be the work of future studies.

ACKNOWLEDGMENTS

The authors thank Dr. Yong Wang for assistant in the ICP measurement. And D.X. acknowledges the University of Melbourne for support through a Melbourne International Engagement Award.

[1] C. Burda, X. Chen, R. Narayanan, and M. A. El-Sayed, Chem. Rev. **105**, 1025 (2005).
[2] K. L. Kelly, E. Coronado, L. L. Zhao, and G. C. Schatz, J. Phys. Chem. B **107**, 668 (2003).
[3] P. H. C. Camargo, K. G. Satyanarayana, and F. Wypych, Materials Res. **12**, 1 (2009).
[4] P. Coussot, *Rheometry of Pastes, Suspensions, and Granular Materials: Applications in Industry and Environment* (John Wiley & Sons, New York, 2005).
[5] Y. Lin, A. Böker, J. He, K. Sill, H. Xiang, C. Abetz, X. Li, J. Wang, T. Emrick, S. Long *et al.*, Nature **434**, 55 (2005).

[6] G. B. Jeffery, Proc. Roy. Soc. London Ser. A: Math. Phys. Character **102**, 161 (1922).
[7] D. Xie, M. Lista, G. G. Qiao, and D. E. Dunstan, J. Phys. Chem. Lett. **6**, 3815 (2015).
[8] A. Tuteja, M. E. Mackay, C. J. Hawker, and B. Van Horn, Macromolecules **38**, 8000 (2005).
[9] M. E. Mackay, T. T. Dao, A. Tuteja, D. L. Ho, B. Van Horn, H.-C. Kim, and C. J. Hawker, Nat. Mater. **2**, 762 (2003).
[10] A. R. Petosa, D. P. Jaisi, I. R. Quevedo, M. Elimelech, and N. Tufenkji, Environ. Sci. Technol. **44**, 6532 (2010).
[11] J. Mewis and N. J. Wagner, J. Non-Newtonian Fluid Mech. **157**, 147 (2009).
[12] G. M. Whitesides and B. Grzybowski, Science **295**, 2418 (2002).
[13] A. Zaccone, H. Wu, D. Gentili, and M. Morbidelli, Phys. Rev. E **80**, 051404 (2009).
[14] D. Xie, H. Wu, A. Zaccone, L. Braun, H. Chen, and M. Morbidelli, Soft Matter **6**, 2692 (2010).
[15] A. Zaccone, D. Gentili, H. Wu, M. Morbidelli, and E. Del Gado, Phys. Rev. Lett. **106**, 138301 (2011).
[16] D. Feke, N. Prabhu, J. Mann Jr, and J. Mann III, J. Phys. Chem. **88**, 5735 (1984).
[17] H. N. Lekkerkerker and R. Tuinier, *Colloids and the Depletion Interaction* (Springer, Berlin, 2011), Vol. 833.
[18] D. H. Napper, *Polymeric Stabilization of Colloidal Dispersions* (Academic Press, San Diego, 1983), Vol. 3.
[19] D. Highgate, Nature **211**, 1390 (1966).
[20] R. Scirocco, J. Vermant, and J. Mewis, J. Non-Newtonian Fluid Mech. **117**, 183 (2004).
[21] J. Michele, R. Pätzold, and R. Donis, Rheol. Acta **16**, 317 (1977).
[22] M. Lyon, D. Mead, R. Elliott, and L. Leal, J. Rheol. **45**, 881 (2001).
[23] M. Jefri and A. Zahed, J. Rheol. **33**, 691 (1989).
[24] J. Feng and D. Joseph, J. Fluid Mech. **324**, 199 (1996).
[25] L. Petit and B. Noetinger, Rheol. Acta **27**, 437 (1988).
[26] D. Won and C. Kim, J. Non-Newtonian Fluid Mech. **117**, 141 (2004).
[27] M. J. Riddle, C. Narvaez, and R. B. Bird, J. Non-Newtonian Fluid Mech. **2**, 23 (1977).
[28] E. Bot, M. Hulsen, and B. Van den Brule, J. Non-Newtonian Fluid Mech. **79**, 191 (1998).
[29] F. Snijkers, R. Pasquino, and J. Vermant, Langmuir **29**, 5701 (2013).
[30] S. J. Gason, D. V. Boger, and D. E. Dunstan, Langmuir **15**, 7446 (1999).
[31] J. R. Stokes, L. J. Graham, N. J. Lawson, and D. V. Boger, J. Fluid Mech. **429**, 67 (2001).
[32] C. F. Bohren and D. R. Huffman, *Absorption and Scattering of Light by Small Particles* (John Wiley & Sons, New York, 2008).
[33] T. Inagaki, E. Arakawa, R. Hamm, and M. Williams, Phys. Rev. B **15**, 3243 (1977).